THE JOURNAL OF PHYSICAL CHEMISTRY C

Article

Cite This: J. Phys. Chem. C 2018, 122, 20358−20365

pubs.acs.org/JPCC

Boron Doping and Defect Engineering of Graphene Aerogels for Ultrasensitive NO_2 Detection

Sally Turner,[□,†,⊥,¶] Wenjun Yan,[□,‡,§] Hu Long,[⊥,¶] Art J. Nelson,[∥] Alex Baker,[∥] Jonathan R. I. Lee,[∥] Carlo Carraro,[‡] Marcus A. Worsley,[∥] Roya Maboudian,[*,‡] and Alex Zettl[*,⊥,¶,#]

[†]Department of Chemistry, [‡]Department of Chemical & Biomolecular Engineering, and Berkeley Sensor & Actuator Center (BSAC), and [⊥]Department of Physics, University of California at Berkeley, Berkeley, California 94720, United States

[§]Smart City Research Center of Zhejiang, Hangzhou Dianzi University, Hangzhou 310018, China

[∥]Physical and Life Sciences Directorate, Lawrence Livermore National Laboratory, Livermore, California 94550, United States

[¶]Kavli Energy Nanoscience Institute at the University of California, Berkeley and the Lawrence Berkeley National Laboratory, Berkeley, California 94720, United States

[#]Materials Sciences Division, Lawrence Berkeley National Laboratory, Berkeley, California 94720, United States

Supporting Information

ABSTRACT: Boron-doped and defect-engineered graphene aerogels are prepared using triphenyl boron as a boron precursor and subsequent heat treatments. The boron chemistry and concentration in the graphene lattice are found to be highly dependent on the temperature used to activate boron. At 1500 °C, boron is incorporated at 3.2 atom % through a combination of B−C, B−N, and B−O bonds. At 1750 °C, the boron concentration decreases to 0.7 atom % and is predominantly incorporated through B−N bonding. Higher temperatures result in complete expulsion of boron from the lattice, leaving behind defects that are found to be beneficial for NO_2 gas detection. The gas sensing properties are explored to gain insight into the impact of boron chemistry on the sensing performance. A highly sensitive and selective conductometric NO_2 sensor is fabricated on a low-power microheater. Defect-engineered graphene aerogels with no boron remaining have superior gas detection properties. At an optimum sensing temperature of 240 °C, the defect-engineered aerogel has a theoretical detection limit of 7 ppb for NO_2 and response and recovery times of 100 and 300 s, respectively, with excellent selectivity over ammonia and hydrogen. The superior gas sensing performance of defect-engineered graphene aerogels has remarkable implications for their performance in catalysis and energy storage applications.

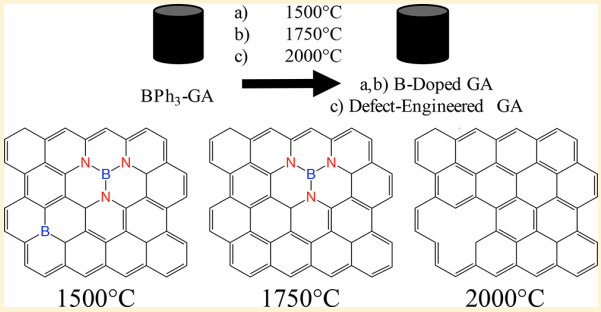

1. INTRODUCTION

Graphene aerogels are an important class of materials made of 2D graphene sheets covalently cross-linked into a 3D structure. These multifunctional materials have low densities and high surface areas and largely retain the extraordinary electrical and thermal properties of their graphene building block.[1−5] The excitement surrounding the potential applications of graphene in supercapacitor and battery electrodes, hydrogen storage, chemical sensing, and water treatment is mirrored in the field of graphene aerogels.[6−11] However, modification of graphene aerogels is necessary to improve their performance for mainstream applications.

Many approaches can be used to alter graphene's electronic structure, with doping being a popular strategy to enhance the electronic and catalytic properties of graphitic materials.[12−16] Two common dopants for graphene are boron and nitrogen due to their similar atomic radii to carbon and ease of substitution. Several theoretical studies report that boron doping of graphene results in improvements in battery, supercapacitor, hydrogen storage, and gas sensing performances.[14,17,18] Not only does the introduction of heteroatoms play a beneficial role, but the introduction of additional defects into the highly crystalline lattice can also be favorable. These two chemical modifications can be particularly advantageous to the performance for molecular gas detection. Theoretical work indicates that boron-doped graphene and defective graphene have superior potential for NO_2 detection due to enhanced adsorption energies and charge transfer from the graphene to NO_2.[18] Experimental work on single layer boron-doped graphene supports these predictions.[19] These promising findings have led researchers to explore doping methods in graphene aerogels.

A large body of research has explored self-assembly methods of graphene oxide (GO) composites by incorporating

Received: June 22, 2018
Revised: August 14, 2018
Published: August 14, 2018

DOI: 10.1021/acs.jpcc.8b05984
J. Phys. Chem. C 2018, 122, 20358−20365

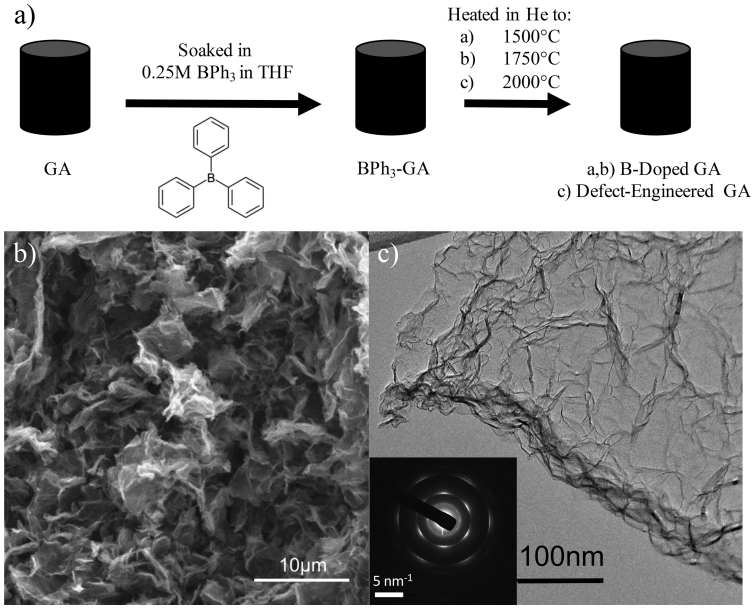

Figure 1. (a) Synthesis of BPh_3−GAs using infiltration and heat treatment. (b, c) SEM and TEM image, with inset diffraction pattern, of BPh_3−GA heated to 2000 °C, respectively.

functional molecules into the synthesis.[20−23] While several studies have used boron and nitrogen incorporation in order to enhance the performance of graphene aerogels for various applications, low temperatures are employed resulting in boron containing functional groups and incomplete reduction of graphene oxide to graphene.[13,24−28] Graphene aerogels are particularly attractive for gas sensing applications due to their high surface area that facilitates the adsorption of a large quantity of gas molecules, resulting in a highly sensitive sensor. Modifications to graphene aerogels for sensing have been largely limited to the introduction of active sensing materials into the high surface area structure of the aerogel, such as nanoparticles or other 2D materials.[29−31]

In this work, we use temperatures as high as 2000 °C with the aim of synthesizing graphene aerogels containing sp^2-bonded boron dopants and extensively characterize the material to validate the sp^2-bonded nature of boron. The temperatures used in this study are also selected for the controlled formation of additional defects. The evolution of boron chemistry with temperature is studied, and the effects of the evolving boron chemistries on the gas sensing properties are investigated in order to fabricate an optimized NO_2 gas sensor using only graphene aerogels as a sensing material. To our knowledge this is the first report of doping and thermal dopant ejection to synthesize defect-engineered graphene aerogels and one of the early reports on the intentional formation of defects within graphene aerogels.[32]

2. EXPERIMENTAL SECTION

2.1. Aerogel Synthesis. *Synthesis of Graphene Aerogels.* Control graphene aerogels are synthesized using a base-catalyzed synthesis reported previously.[3] Briefly, a 20 mg/mL solution of GO in water is sonicated, and a 1:6 by volume NH_4OH:H_2O is added to catalyze the gelation. Gelation is carried out over 3 days at 80 °C. After gelation, the solvent in the hydrogel is removed using supercritical carbon dioxide to yield a graphene oxide aerogel. Thermal reduction is achieved by treatment at 1050 °C in Ar and subsequent treatment at either 1500, 1750, or 2000 °C to yield control graphene aerogels (GA).

Synthesis of BPh_3−GA Samples. Control graphene aerogels reduced at 1050 °C are immersed in a solution of 0.25 M triphenyl borane (BPh_3) in THF under argon protection overnight. The solution is evaporated, and the BPh_3-infiltrated GA is annealed at either 1500, 1750, or 2000 °C in He to yield BPh_3−GA samples.

2.2. Gas Sensing. *Sensor Fabrication.* The microheater is fabricated according to the process in a previous report.[6] A silicon substrate is coated with silicon-rich, low-stress silicon nitride (100 nm) followed by the deposition of phosphorus-doped polysilicon (100 nm), which is patterned using photolithography to form the microheater. Another silicon nitride layer (100 nm) is deposited and patterned for the microheater contacts, which are electron-beam-evaporated Ti/Pt (10/90 nm). The back side of the wafer is patterned and etched using KOH to release the silicon nitride membrane. The Ti/Pt electrodes overlaid on the silicon nitride membrane are used as electrodes for conductometric sensing. The chip is wire bonded into a 14-pin ceramic dual inline package for electrical characterization and sensor testing. Conductometric gas sensors are prepared by integrating a BPh_3−GA onto the low-power microfabricated heater platform. The aerogel is sonicated into suspension in isopropyl alcohol (0.5 mg/mL). A 1 μL drop (five drops of 0.2 μL each) is placed onto the microheater chip, while the microheater is heated to 100 °C and maintained there for 3 h to promote solvent evaporation and material deposition at the center of the microheater.

Sensing Testing. For sensor testing, the sensor is placed in a gas flow chamber (~1 cm^3 volume). Gas exposure and signal collection are controlled using Labview and an open-source Java-based instrument and control and measurement software suite, Zephyr. Different gas streams are controlled with mass flow controllers (Bronkhurst) to give the desired gas concentration with a total flow rate of 300 sccm. For sensor

DOI: 10.1021/acs.jpcc.8b05984
J. Phys. Chem. C 2018, 122, 20358−20365

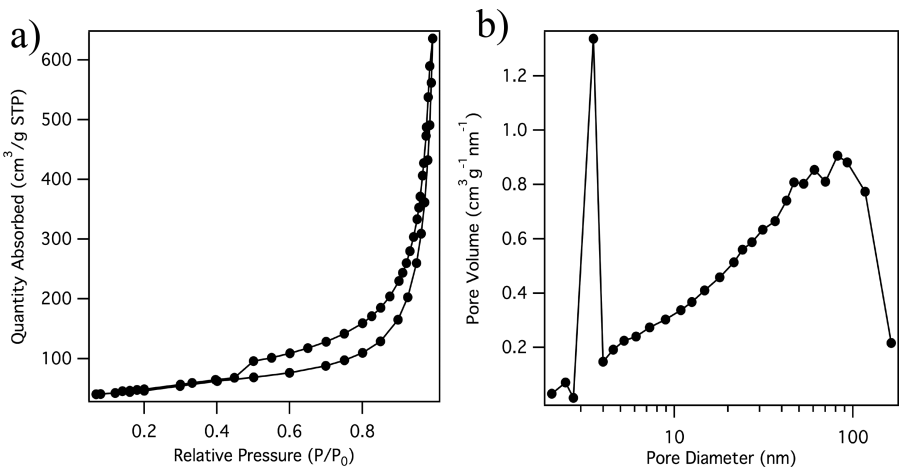

Figure 2. (a, b) N_2 adsorption−desorption isotherms and pore size distribution for BPh_3−GA heated to 2000 °C, respectively.

signal collection, a bias voltage is applied to the sensing electrodes, and the sensor's resistance is measured with a Keithley 2602A source-meter.

3. RESULTS AND DISCUSSION

3.1. BPh_3−GA Synthesis and Characterization. BPh_3 is selected as a doping precursor due to the similarities in the structure to the desired substitutional doping product. As shown in Figure 1a, after synthesis of a graphene aerogel, it is submerged in a solution of triphenyl borane and allowed to dry. The infiltrated aerogel is then fired at 1500, 1750, or 2000 °C to provide enough thermal energy to drive boron into the graphene lattice. The resulting changes in morphology, boron chemistries, concentrations, and sensing performance to NO_2 are monitored.

The morphology of BPh_3−GA is characterized using scanning electron microscopy (SEM) and transmission electron microscopy (TEM) to probe possible structural changes at the micro- and nanoscale. In Figure 1b, a representative SEM image of a BPh_3−GA fired at 2000 °C is shown. The morphology after infiltration is unchanged, and the open porous structure is maintained. This retention of morphology is independent of temperature used for firing (Figure S1). TEM analysis shows the traditional wrinkled structure characteristic of graphene aerogels (Figure 1c) with a hexagonal diffraction pattern (inset) and lattice spacing of 0.39 nm, close to the ideal spacing for graphene (0.33 nm). The BPh_3−GA samples fired at 1500, 1750, and 2000 °C have similar 3D and wrinkled morphology, and no flattening on the scale of around 20 nm is observed with increasing annealing temperature, consistent with previous reports[3] (Figure S2). Overall, no change in morphology at the nanoscale or microscale is observed as a function of annealing temperature.

High surface area and porosity are important properties of graphene aerogels and vital to many of their functionalities. The nitrogen adsorption/desorption isotherm for a 2000 °C fired BPh_3−GA is shown in Figure 2a displaying a type-IV hysteresis loop (IUPAC definition) typical of mesoporous materials. The calculated BET surface area for BPh_3−GA fired at 2000 °C is about 160 m^2/g, which is smaller than control graphene aerogels (~1000 m^2/g). The reduced surface area is likely due to surface tension effects during THF evaporation after infiltration of BPh_3. While there is a decrease in the surface area as a result of the BPh_3−GA, the resulting aerogel still possesses a high surface area and pore volume sufficient for many applications. The pore size distribution shown in Figure 2b has a strong peak at about 3.5 nm and a tail into the larger pore regime reflecting the large surface area of the BPh_3−GA.

In order to characterize crystallinity, boron concentration, and boron chemistries in the graphene aerogel after the firing process, Raman spectroscopy, X-ray photoelectron spectroscopy (XPS), and X-ray absorption spectroscopy (XAS) are utilized. Raman spectroscopy is a powerful tool to study graphene and gives insight into the crystallinity and defect concentration in the material. The Raman spectrum of graphene has a G peak corresponding to the in-plane E_{2g} phonon around 1590 cm^{-1}, a second-order two-phonon mode identified as the 2D peak at 2700 cm^{-1}, and a D peak due to defects in the material at 1350 cm^{-1}. The ratio of the intensity of the D peak to the G peak (I_D/I_G) is a common metric for evaluating the quality of graphene. Introduction of a heteroatom into the lattice would increase the D to G ratio, and it has been used as an indicator of doping levels.[33] Figures 3 a, b contain the Raman spectra of BPh_3−GA and GA samples, fired at various temperatures. For GA samples, a decrease in I_D/I_G and sharpening of the G peak is observed with increased firing temperature. These trends and I_D/I_G values measured are in agreement with previous work.[3] This behavior is mirrored in BPh_3−GA samples, but the I_D/I_G is increased at all heat treatments when compared to GA samples. At 1500 and 1750 °C firing temperatures, I_D/I_G in BPh_3−GA increases by 21% and 14% relative to the control, respectively. The largest increase occurs at 2000 °C for which the BPh_3−GA has a I_D/I_G 58% larger than the control, indicating that there is an increased number of defects after BPh_3 treatment.

In order to determine if the increased defects in the BPh_3−GA samples are due to incorporation of boron, XPS and XAS are performed. Boron 1s XPS spectra for aerogels fired at 1500, 1750, and 2000 °C are shown in Figure 3c. A clear trend is present in the atomic concentration of boron incorporated. At 1500 °C, boron is incorporated at 3.2 atom %; after firing at 1750 °C the boron level drops to 0.7%; and after the 2000 °C treatment no detectable boron remains in the lattice. Importantly, bonds that incorporate boron into the material vary with temperature. After firing at 1500 °C, boron is

DOI: 10.1021/acs.jpcc.8b05984
J. Phys. Chem. C 2018, 122, 20358−20365

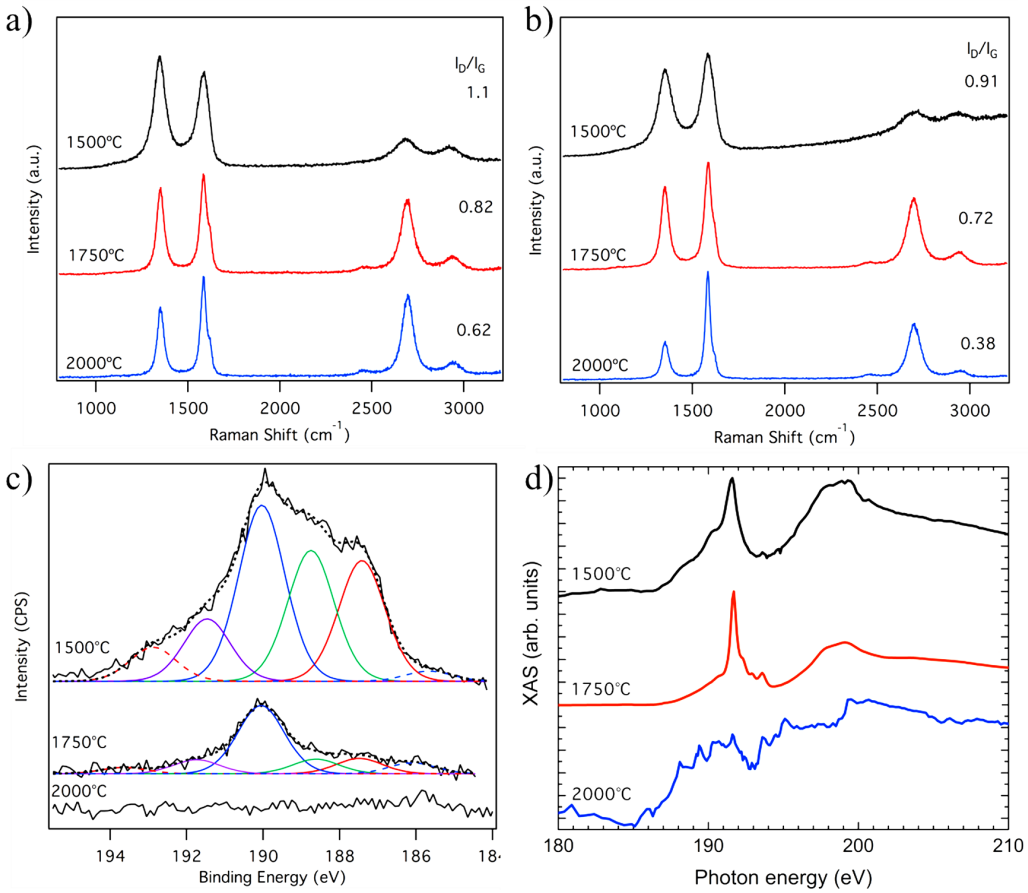

Figure 3. (a, b) Raman spectra of BPh_3−GAs and GAs fired at increasing temperatures, respectively. (c) B 1s XPS spectra of BPh_3−GAs fired at increasing temperatures. (d) XAS spectra for BPh_3−GAs fired at increased temperature. Spectra normalized and offset for clarity.

incorporated through B_2O_3, BC_2O, BN, BC_2N/BN_2C, BC_3, and B−B bonds indicated by peaks at 192.9, 191.5, 190.1, 188.8, 187.4, and 185.6 eV, respectively. Given that graphene oxide is used as a precursor, the presence of boron and oxygen bonding is not surprising. However, no nitrogen source is used in the BPh_3−GA samples that is not present in the control, making B−N bonding unexpected. BN is known to be a thermodynamically favorable phase, and the source of nitrogen in this case is likely due to nitrogen in the air present in the aerogel pores.[34] At 1750 °C there is a change in the boron chemistry, and B−N is the predominant source of boron incorporation. Aerogels fired at 2000 °C have no detectable boron which we attribute to boron being annealed out and expelled from the lattice at such high temperatures through a self-healing mechanism.[35,36] Changes in boron chemistries are summarized in Table S1. Additionally, at such low doping levels no change in the carbon spectrum is visible (Figure S3).

As a highly sensitive tool to characterize the element-specific local bonding environment, XAS is used to determine if boron is incorporated into the lattice of the BPh_3−GA samples through sp^2 bonds or simply resides within a functional group on the surface through sp^3 bonds. The boron XAS spectrum is shown in Figure 3d. Two important features appear at 191.7 and 193.6 eV; these arise from sp^2-hybridized boron bonded to nitrogen and oxygen, respectively. Comparison of the B, C, and N spectra against previous studies confirms the incorporation of B and N as dopants, rather than forming isolated regions of B_4C or hBN (Figure S4).[37,38] At 1500 °C, the B−N π^* peak at 191.7 eV dominates, but a smaller feature is also observed at 190.5 eV, which is attributed to substitutional doping of boron in an sp^2-hybridized, $B-C_3$ environment.[38] Additionally, a small peak at 193.6 eV is present due to the oxidized species on the surface. Aerogels fired at 1750 °C have a similar dominant peak at 191.7 eV, but there is a decrease in the relative intensity of the $B-C_3$ features, in agreement with XPS data. There is also an increase in surface oxide species, as the oxidized boron peak increases in prominence. The BPh_3−GA sample fired at 2000 °C displays dramatically reduced signal strength, and consequently no clear structure can be resolved.

Each method provides complementary information in providing a clear picture of the evolution of boron incorporation with annealing temperature. The BPh_3−GA samples fired at 1500 °C have boron incorporation through similar levels of B−N and B−C bonding, with additional oxidized boron. Aerogels fired at 1750 °C have an overall decreased level of boron incorporated, and the incorporation is predominantly through B−N bonds. Importantly, boron is bound in the material through substitutional doping via sp^2 bonds as opposed to boron functional groups on the surface. Finally, the BPh_3−GA samples treated at 2000 °C contain no detectable boron. However, Raman spectroscopy indicates that this material has an increased density of defects. These defects

DOI: 10.1021/acs.jpcc.8b05984
J. Phys. Chem. C 2018, 122, 20358−20365

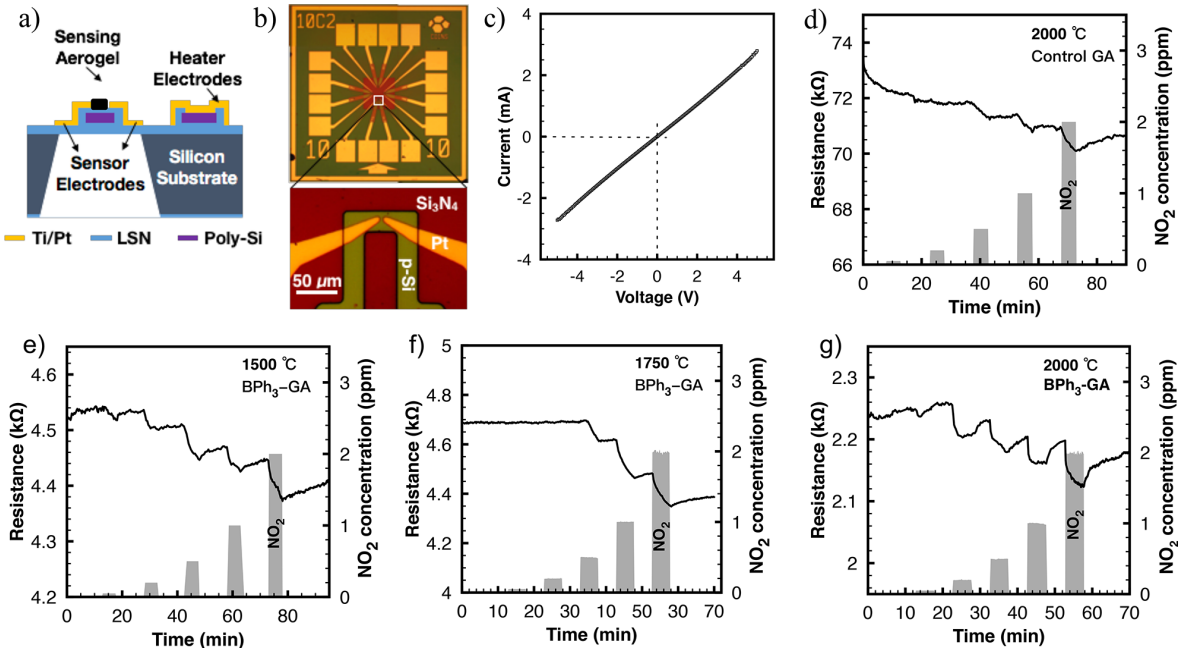

Figure 4. (a) Schematic diagram of the sensor cross section. (b) Optical image of a 3.5 × 3.5 mm^2 chip containing four microheaters and zoom-in of one microheater with sensing electrodes on top. (c) *I*/*V* characteristics of the BPh_3–GA (heated to 2000 °C) sensor at RT. Resistance versus time to NO_2 (0.05–2 ppm range) at RT of the sensors based on (d) GA, (e) BPh_3–GA heated at 1500 °C, (f) BPh_3–GA heated at 1750 °C, and (g) BPh_3–GA heated at 2000 °C.

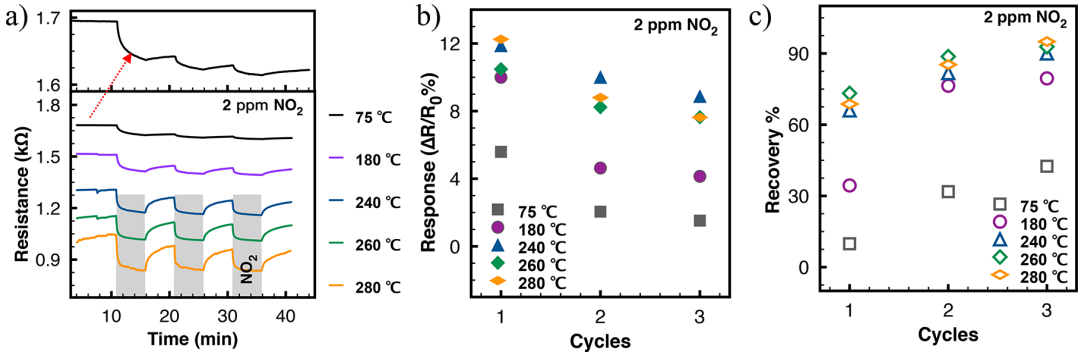

Figure 5. (a) Resistance change of the 2000 °C BPh_3–GA sensor, (b) % response change, and (c) % recovery change during 3 cyclic exposures to 2 ppm of NO_2 at different microheater temperatures.

can serve as active sites for catalysis and gas sensing and provide a route toward defect-engineering of graphene aerogels.

3.2. Gas Sensing Performance. The gas sensing properties of aerogels with different boron chemistries are explored by preparing aerogels on a low-power microheater chip shown in Figure 4a. A microheater chip (3.5 × 3.5 mm^2) contains four microheater sensors, with each sensor having four electrical contacts, two for the microheater leads and two for electrical probing of the sensing layer (Figure 4b). Taking the 2000 °C BPh_3–GA sample as an example, nearly linear current vs voltage behavior of the BPh_3–GA sensor suggests an ohmic contact between the aerogel and sensor electrode (Figure 4c). Figures 4d–g and Table S2 show the responses of GA and BPh_3–GA sensors to different concentrations of NO_2 at room temperature (20 °C) for 5 min duration pulses. There is a clear change in the sensing performance for BPh_3–GA materials fired at different temperatures. The resistance of all sensors decreases upon exposure to NO_2 gas, demonstrating a p-type behavior, in agreement with experimental and theoretical findings of NO_2 on graphene.[29,39] Notably, the GA is unable to detect NO_2 concentrations below 0.5 ppm and has a response of 2.6% to 2 ppm of NO_2. The sensors based on BPh_3–GA annealed at 1500 °C have an enhanced detection limit and respond to concentrations as low as 0.05 ppm of NO_2 with the same signal response to 2 ppm of NO_2 as the control. The sensors based on 1750 °C BPh_3–GA have a detection limit the same as the control but have an enhanced response to 2 ppm of NO_2 with a 4.6% change in resistance. Lastly, the sensors based on BPh_3–GA annealed at 2000 °C detect NO_2 concentrations of 0.05 ppm, a factor of 10 enhancement with respect to the control. Additionally, the response of the material is improved threefold and has an 8% change in resistance to 2 ppm of NO_2. The changes in sensing

DOI: 10.1021/acs.jpcc.8b05984
J. Phys. Chem. C 2018, 122, 20358–20365

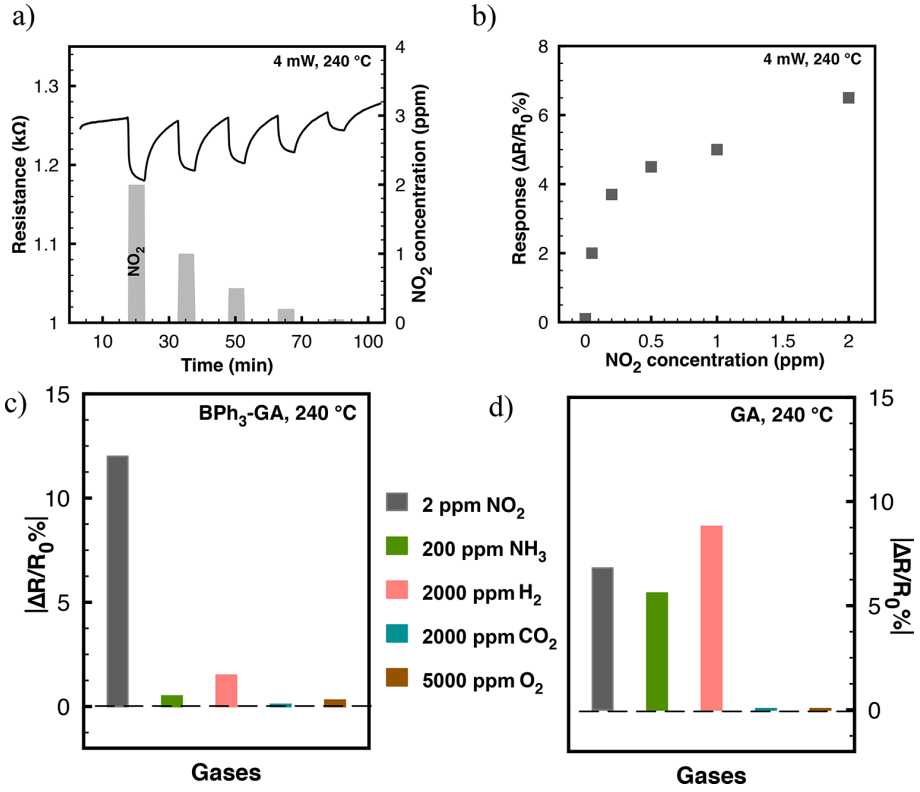

Figure 6. (a) Resistance versus time and (b) % response of the 2000 °C BPh_3−GA sensor to NO_2 at 240 °C. The NO_2 concentration was modulated decreasing from 2 to 0.05 ppm. (c, d) Selectivity of the 2000 °C BPh_3−GA sensor and GA sensor at 240 °C, respectively.

performance may be attributed to the distinct boron chemistries or defects left behind as a result of BPh_3 treatment. Boron incorporated through substitutional doping via $B-C_3$ bonds yields active sites for NO_2 adsorption.[18] Thus, the 1500 °C BPh_3−GA, which contains 23% B incorporation through $B-C_3$ bonds and 33% through $B-N_3$, has a decreased detection limit. Boron incorporation through B−N bonds is not thought to be beneficial to sensing performance, and the effect of BC_2N/BN_2C is unknown. Therefore, the predominant B incorporation through 53% B−N bonds in the 1750 °C BPh_3−GA is not contributing to sensing, and the detection limit is not enhanced. The BPh_3−GA treated at 2000 °C has no detectable boron but rather an increased density of defects left behind due to boron expulsion from the lattice. These defects are active sites for NO_2 adsorption and contribute to the sensing behavior of the material, making defect-engineered aerogels excellent NO_2 sensors. Due to the enhanced detection limit and sensitivity of defect-engineered BPh_3−GA, the sensors based on 2000 °C BPh_3−GA are further characterized.

The effect of heater temperature on the 2000 °C BPh_3−GA sensor is reported in Figure 5. Figure 5a displays the response of the sensor during exposure to 2 ppm of NO_2 for 3 cycles, with the temperature of the chip ranging from 70 to 280 °C. When exposed to 2 ppm of NO_2 flow, the percentage response decreases after repeating the three sensing cycles, for all temperatures, while the percentage recovery increases with increased temperature (Figure 5b,c). Due to the high binding energy of NO_2 on the defect-engineered GA, the binding sites become tightly occupied by NO_2 molecules after adsorption. At lower temperatures, the thermal energy is insufficient to overcome the activation energy for NO_2 desorption. Therefore, as the adsorption/desorption cycles are repeated, the initial resistance is reduced as a result of nonrecoverable response. Additionally, as the temperature increases from 70 to 240 °C, the percentage response of the sensor increases, and the recovery characteristics improve. This is due to the high temperature accelerating the adsorption and desorption of NO_2 gas molecules on the aerogel surface. However, in the temperature range of 240−280 °C, both the response and recovery changes are slight, with response time around 100 s and recovery time around 300 s. Considering the response and recovery characteristics to NO_2 and the power consumption of the device, a sensor temperature of 240 °C is considered the optimum operating temperature, and further tests are taken at this sensing temperature.

The 2000 °C BPh_3−GA sensor response to varied concentrations of NO_2 from 0.05 to 2 ppm at 240 °C is shown in Figures 6a and 6b. The sensor response is clearly detectable at extremely low concentrations of 50 ppb and exhibits minimal noise. Although the minimum NO_2 delivery concentration is 50 ppb due to limitations with the experimental setup, the detection limit of the BPh_3−GA sensor based on the signal-to-noise ratio of 3 is estimated at 7 ppb.[40] Additionally, the sensor has fast response and recovery times for all NO_2 concentrations between 90 and 120 and 300 s, respectively.

The most remarkable benefit of defect engineering is the improved selectivity to NO_2, compared to the GA. As shown in Figure 6c, the 2000 °C BPh_3−GA sensor shows excellent selectivity to NO_2 at a much lower concentration (2 ppm),

DOI: 10.1021/acs.jpcc.8b05984
J. Phys. Chem. C 2018, 122, 20358−20365

with a weak response to higher concentrations of NH_3 and H_2. In contrast, the GA sensor does not exhibit such high selectivity as it responds to H_2, NH_3, and NO_2, with the highest response percentage to 2000 ppm of H_2 at 240 °C (Figure 6d). Based on first-principles calculations, the introduction of defects into the aerogel results in a binding affinity for NO_2 12 and 6 times larger than for NH_3 and H_2, respectively, resulting in more favorable adsorption and selectivity for NO_2 than other gases.[18,41]

4. CONCLUSION

In conclusion, boron-doped and defect-engineered graphene aerogels are synthesized using triphenyl borane as a precursor and subsequent heat treatments. High-temperature firing at 1500 and 1750 °C yields boron-doped graphene aerogels, and firing at 2000 °C produces graphene aerogels with enhanced defects. Conductometric gas sensors are fabricated using B-doped and defect-engineered aerogels as the active sensing material. While all aerogels have superior gas sensing performance to NO_2 compared to control graphene aerogels, defect-engineered aerogels have the greatest performance enhancement. At an optimum sensing temperature of 240 °C, the defect-engineered aerogel has a theoretical detection limit of 7 ppb and response and recovery times of 100 and 300 s, respectively, with remarkable selectivity for NO_2 over ammonia and hydrogen. Defect-engineered aerogels are expected to have enhanced performance for numerous other applications including catalysis due to the increased number of active sites.

■ ASSOCIATED CONTENT

Supporting Information

The Supporting Information is available free of charge on the ACS Publications website at DOI: 10.1021/acs.jpcc.8b05984.

Additional characterization and sensing in an inert environment (PDF)

■ AUTHOR INFORMATION

Corresponding Authors

*E-mail: azettl@berkeley.edu.

*E-mail: maboudia@berkeley.edu.

ORCID

Sally Turner: 0000-0003-0618-5133

Carlo Carraro: 0000-0002-3482-9226

Author Contributions

□S.T. and W.Y. contributed equally to this work.

Author Contributions

S.T. and W.Y. prepared the manuscript. S.T. synthesized aerogels and provided characterization. A.J.N., J.R.I.L., A.B., H.L., and C.C. provided additional characterizations. W.Y. conducted sensing experiments. All authors have given approval to the final version of the manuscript.

Notes

The authors declare no competing financial interest.

■ ACKNOWLEDGMENTS

S.T. and W.Y. contributed equally to this work. This work was supported in part by the Director, Office of Science, Office of Basic Energy Sciences, Materials Sciences, and Engineering Division, of the U.S. Department of Energy under Contract No. DE-AC02-05-CH11231, within the sp^2-Bonded Materials Program (KC2207) (TEM and SEM characterization); by the Air Force Office of Scientific Research under Award No. FA9550-14-1-0323 (synthesis); by BSAC industrial members (sensor fabrication and characterization); and at LLNL under the auspices of the U.S. Department of Energy under contract No. DE-AC52-07NA27344 (supplementary synthesis and structural characterization). XAS measurements described in this paper were performed at the CLS on the REIXS beamline BL10ID-2, which is supported by the Canada Foundation for Innovation, Natural Sciences, and Engineering Research Council of Canada, the University of Saskatchewan, the Government of Saskatchewan, Western Economic Diversification Canada, the National Research Council Canada, and the Canadian Institutes of Health Research. The views and opinions of the authors expressed herein do not necessarily state or reflect those of the United States Government or any agency thereof. Neither the United States Government nor any agency thereof, nor any of their employees, makes any warranty, expressed or implied, or assumes any legal liability or responsibility for the accuracy, completeness, nor usefulness of any information, apparatus, product, or process disclosed, or represents that its use would not infringe privately owned rights. S.T. and W.Y. acknowledge support from an NSF GRFP Fellowship and a Chinese Scholarship Council Fellowship, respectively.

■ REFERENCES

(1) Worsley, M. A.; Charnvanichborikarn, S.; Montalvo, E.; Shin, S. J.; Tylski, E. D.; Lewicki, J. P.; Nelson, A. J.; Satcher, J. H.; Biener, J.; Baumann, T. F.; Kucheyev, S. O. Toward Macroscale, Isotropic Carbons with Graphene-Sheet-Like Electrical and Mechanical Properties. *Adv. Funct. Mater.* **2014**, *24*, 4259−4264.

(2) Worsley, M. A.; Pauzauskie, P. J.; Olson, T. Y.; Biener, J.; Satcher, J. H.; Baumann, T. F. Synthesis of Graphene Aerogel with High Electrical Conductivity. *J. Am. Chem. Soc.* **2010**, *132*, 14067−14069.

(3) Worsley, M. A.; Pham, T. T.; Yan, A.; Shin, S. J.; Lee, J. R. I.; Bagge-Hansen, M.; Mickelson, W.; Zettl, A. Synthesis and Characterization of Highly Crystalline Graphene Aerogels. *ACS Nano* **2014**, *8*, 11013−11022.

(4) Huang, H.; Chen, P.; Zhang, X.; Lu, Y.; Zhan, W. Edge-to-Edge Assembled Graphene Oxide Aerogels with Outstanding Mechanical Performance and Superhigh Chemical Activity. *Small* **2013**, *9*, 1397−1404.

(5) Zhang, X.; Sui, Z.; Xu, B.; Yue, S.; Luo, Y.; Zhan, W.; Liu, B.; Lima, M. D.; Haque, M. H.; Gartstein, Y. N. Mechanically Strong and Highly Conductive Graphene Aerogel and Its Use as Electrodes for Electrochemical Power Sources. *J. Mater. Chem.* **2011**, *21*, 6494−6497.

(6) Harley-Trochimczyk, A.; Chang, J.; Zhou, Q.; Dong, J.; Pham, T.; Worsley, M. A.; Maboudian, R.; Zettl, A.; Mickelson, W. Catalytic Hydrogen Sensing Using Microheated Platinum Nanoparticle-Loaded Graphene Aerogel. *Sens. Actuators, B* **2015**, *206*, 399−406.

(7) Sui, Z.; Meng, Q.; Zhang, X.; Ma, R.; Cao, B. Green Synthesis of Carbon Nanotube−Graphene Hybrid Aerogels and Their Use as Versatile Agents for Water Purification. *J. Mater. Chem.* **2012**, *22*, 8767−8771.

(8) Ye, S.; Feng, J.; Wu, P. Deposition of Three-Dimensional Graphene Aerogel on Nickel Foam as a Binder-Free Supercapacitor Electrode. *ACS Appl. Mater. Interfaces* **2013**, *5*, 7122−7129.

(9) Kabbour, H.; Baumann, T.; Satcher, J.; Saulnier, A.; Ahn, C. Toward New Candidates for Hydrogen Storage: High-Surface-Area Carbon Aerogels. *Chem. Mater.* **2006**, *18*, 6085−6087.

(10) Xiao, J.; Mei, D.; Li, X.; Xu, W.; Wang, D.; Graff, G. L.; Bennett, W. D.; Nie, Z.; Saraf, L. V.; Aksay, I. A.; Liu, J.; Zhang, J.-G.

Hierarchically Porous Graphene as a Lithium−Air Battery Electrode. *Nano Lett.* **2011**, *11*, 5071−5078.
(11) Zhu, Y.; Murali, S.; Stoller, M. D.; Ganesh, K. J.; Cai, W.; Ferreira, P. J.; Pirkle, A.; Wallace, R. M.; Cychosz, K. A.; Thommes, M.; Su, D.; Stach, E. A.; Ruoff, R. S. Carbon-Based Supercapacitors Produced by Activation of Graphene. *Science* **2011**, *332*, 1537−1541.
(12) Zhao, Y.; Yang, L.; Chen, S.; Wang, X.; Ma, Y.; Wu, Q.; Jiang, Y.; Qian, W.; Hu, Z. Can Boron and Nitrogen Co-Doping Improve Oxygen Reduction Reaction Activity of Carbon Nanotubes? *J. Am. Chem. Soc.* **2013**, *135*, 1201−1204.
(13) Gong, Y.; Fei, H.; Zou, X.; Zhou, W.; Yang, S.; Ye, G.; Liu, Z.; Peng, Z.; Lou, J.; Vajtai, R.; Yakobson, B. I.; Tour, J. M.; Ajayan, P. M. Boron- and Nitrogen-Substituted Graphene Nanoribbons as Efficient Catalysts for Oxygen Reduction Reaction. *Chem. Mater.* **2015**, *27*, 1181−1186.
(14) Jiang, H. R.; Zhao, T. S.; Shi, L.; Tan, P.; An, L. First-Principles Study of Nitrogen-, Boron-Doped Graphene and Co-Doped Graphene as the Potential Catalysts in Nonaqueous Li−O_2 Batteries. *J. Phys. Chem. C* **2016**, *120*, 6612−6618.
(15) Panchakarla, L. S.; Subrahmanyam, K. S.; Saha, S. K.; Govindaraj, A.; Krishnamurthy, H. R.; Waghmare, U. V.; Rao, C. N. R. Synthesis, Structure, and Properties of Boron- and Nitrogen-Doped Graphene. *Adv. Mater.* **2009**, *21*, 4726−4730.
(16) Qu, L.; Liu, Y.; Baek, J.-B.; Dai, L. Nitrogen-Doped Graphene as Efficient Metal-Free Electrocatalyst for Oxygen Reduction in Fuel Cells. *ACS Nano* **2010**, *4*, 1321−1326.
(17) Zhou, Y. G.; Zu, X. T.; Gao, F.; Nie, J. L.; Xiao, H. Y. Adsorption of Hydrogen on Boron-Doped Graphene: A First-Principles Prediction. *J. Appl. Phys.* **2009**, *105*, 014309−014313.
(18) Zhang, Y. H.; Chen, Y. B.; Zhou, K. G.; Liu, C. H.; Zeng, J.; Zhang, H. L.; Peng, Y. Improving Gas Sensing Properties of Graphene by Introducing Dopants and Defects: A First-Principles Study. *Nanotechnology* **2009**, *20*, 185504−185516.
(19) Lv, R.; Chen, G.; Li, Q.; McCreary, A.; Botello-Méndez, A.; Morozov, S. V.; Liang, L.; Declerck, X.; Perea-López, N.; Cullen, D. A.; et al. Ultrasensitive Gas Detection of Large-Area Boron-Doped Graphene. *Proc. Natl. Acad. Sci. U. S. A.* **2015**, *112*, 14527−14532.
(20) Guo, R.; Jiao, T.; Li, R.; Chen, Y.; Guo, W.; Zhang, L.; Zhou, J.; Zhang, Q.; Peng, Q. Sandwiched Fe_3O_4 /Carboxylate Graphene Oxide Nanostructures Constructed by Layer-by-Layer Assembly for Highly Efficient and Magnetically Recyclable Dye Removal. *ACS Sustainable Chem. Eng.* **2018**, *6*, 1279−1288.
(21) Liu, Y.; Hou, C.; Jiao, T.; Song, J.; Zhang, X.; Xing, R.; Zhou, J.; Zhang, L.; Peng, Q. Self-Assembled AgNP-Containing Nanocomposites Constructed by Electrospinning as Efficient Dye Photocatalyst Materials for Wastewater Treatment. *Nanomaterials* **2018**, *8*, 35−49.
(22) Luo, X.; Ma, K.; Jiao, T.; Xing, R.; Zhang, L.; Zhou, J.; Li, B. Graphene Oxide-Polymer Composite Langmuir Films Constructed by Interfacial Thiol-Ene Photopolymerization. *Nanoscale Res. Lett.* **2017**, *12*, 99.
(23) Xu, Y.; Sheng, K.; Li, C.; Shi, G. Self-Assembled Graphene Hydrogel *via* a One-Step Hydrothermal Process. *ACS Nano* **2010**, *4*, 4324−4330.
(24) Zuo, Z.; Jiang, Z.; Manthiram, A. Porous B-Doped Graphene Inspired by Fried-Ice for Supercapacitors and Metal-Free Catalysts. *J. Mater. Chem. A* **2013**, *1*, 13476−13483.
(25) Wang, Z.; Cao, X.; Ping, J.; Wang, Y.; Lin, T.; Huang, X.; Ma, Q.; Wang, F.; He, C.; Zhang, H. Electrochemical Doping of Three-Dimensional Graphene Networks Used as Efficient Electrocatalysts for Oxygen Reduction Reaction. *Nanoscale* **2015**, *7*, 9394−9398.
(26) Tai, J.; Hu, J.; Chen, Z.; Lu, H. Two-Step Synthesis of Boron and Nitrogen Co-Doped Graphene as a Synergistically Enhanced Catalyst for the Oxygen Reduction Reaction. *RSC Adv.* **2014**, *4*, 61437−61443.
(27) Jin, J.; Pan, F.; Jiang, L.; Fu, X.; Liang, A.; Wei, Z.; Zhang, J.; Sun, G. Catalyst-Free Synthesis of Crumpled Boron and Nitrogen Co-Doped Graphite Layers with Tunable Bond Structure for Oxygen Reduction Reaction. *ACS Nano* **2014**, *8*, 3313−3321.
(28) Xie, Y.; Meng, Z.; Cai, T.; Han, W. Q. Effect of Boron-Doping on the Graphene Aerogel Used as Cathode for the Lithium−Sulfur Battery. *ACS Appl. Mater. Interfaces* **2015**, *7*, 25202−25210.
(29) Schedin, F.; Geim, A. K.; Morozov, S. V.; Hill, E. W.; Blake, P.; Katsnelson, M. I.; Novoselov, K. S. Detection of Individual Gas Molecules Adsorbed on Graphene. *Nat. Mater.* **2007**, *6*, 652−655.
(30) Liu, X.; Li, J.; Sun, J.; Zhang, X. 3D Fe_3O_4 Nanoparticle/Graphene Aerogel for NO_2 Sensing at Room Temperature. *RSC Adv.* **2015**, *5*, 73699−73704.
(31) Long, H.; Harley-Trochimczyk, A.; Pham, T.; Tang, Z.; Shi, T.; Zettl, A.; Carraro, C.; Worsley, M. A.; Maboudian, R. High Surface Area MoS_2/Graphene Hybrid Aerogel for Ultrasensitive NO_2 Detection. *Adv. Funct. Mater.* **2016**, *26*, 5158−5165.
(32) Ye, J. C.; Charnvanichborikarn, S.; Worsley, M. A.; Kucheyev, S. O.; Wood, B. C.; Wang, Y. M. Enhanced Electrochemical Performance of Ion-Beam-Treated 3D Graphene Aerogels for Lithium Ion Batteries. *Carbon* **2015**, *85*, 269−278.
(33) Kim, Y. A.; Fujisawa, K.; Muramatsu, H.; Hayashi, T.; Endo, M.; Fujimori, T.; Kaneko, K.; Terrones, M.; Behrends, J.; Eckmann, A.; et al. Raman Spectroscopy of Boron-Doped Single-Layer Graphene. *ACS Nano* **2012**, *6*, 6293−6300.
(34) Yuge, K. Phase Stability of Boron Carbon Nitride in a Heterographene Structure: A First-Principles Study. *Phys. Rev. B: Condens. Matter Mater. Phys.* **2009**, *79*, 144109−144115.
(35) Chen, J.; Shi, T.; Cai, T.; Xu, T.; Sun, L.; Wu, X.; Yu, D. Self Healing of Defected Graphene. *Appl. Phys. Lett.* **2013**, *102*, 103107−1126.
(36) Botari, T.; Paupitz, R.; Alves da Silva Autreto, P.; Galvao, D. S. Graphene Healing Mechanisms: A Theoretical Investigation. *Carbon* **2016**, *99*, 302−309.
(37) McDougall, N. L.; Nicholls, R. J.; Partridge, J. G.; McCulloch, D. G. The Near Edge Structure of Hexagonal Boron Nitride. *Microsc. Microanal.* **2014**, *20*, 1053−1059.
(38) Hanafusa, A.; Muramatsu, Y.; Kaburagi, Y.; Yoshida, A.; Hishiyama, Y.; Yang, W.; Denlinger, J. D.; Gullikson, E. M. Local Structure Analysis of Boron-Doped Graphite by Soft X-Ray Emission and Absorption Spectroscopy Using Synchrotron Radiation. *J. Appl. Phys.* **2011**, *110*, 053504−053509.
(39) Wehling, T.; Novoselov, K.; Morozov, S.; Vdovin, E.; Katsnelson, K.; Geim, A.; Lichtenstein, A. Molecular Doping of Graphene. *Nano Lett.* **2008**, *8*, 173−177.
(40) Dua, V.; Surwade, S. P.; Ammu, S.; Agnihotra, S. R.; Jain, S.; Roberts, K. E.; Park, S.; Ruoff, R. S.; Manohar, S. K. All-Organic Vapor Sensor Using Inkjet-Printed Reduced Graphene Oxide. *Angew. Chem., Int. Ed.* **2010**, *49*, 2154−2157.
(41) Yadav, S.; Zhu, Z.; Singh, C. V. Defect Engineering of Graphene for Effective Hydrogen Storage. *Int. J. Hydrogen Energy* **2014**, *39*, 4981−4995.

DOI: 10.1021/acs.jpcc.8b05984
J. Phys. Chem. C 2018, 122, 20358−20365